Editors' Suggestion

Mechanically Modulated Sideband and Squeezing Effects of Membrane Resonators

Fan Yang,[1] Mengqi Fu,[1] Bojan Bosnjak,[2] Robert H. Blick,[2] Yuxuan Jiang,[3,*] and Elke Scheer[1,†]
[1]Fachbereich Physik, Universität Konstanz, 78457 Konstanz, Germany
[2]Center for Hybrid Nanostructures, Universität Hamburg, 22761 Hamburg, Germany
[3]School of Physics and Optoelectronics Engineering, Anhui University, 230601 Hefei, China

(Received 19 July 2021; revised 2 September 2021; accepted 27 September 2021; published 26 October 2021)

We investigate the sideband spectra of a driven nonlinear mode with its eigenfrequency being modulated at a low frequency (< 1 kHz). This additional parametric modulation leads to prominent antiresonance line shapes in the sideband spectra, which can be controlled through the vibration state of the driven mode. We also establish a direct connection between the antiresonance frequency and the squeezing of thermal fluctuation in the system. Our Letter not only provides a simple and robust method for squeezing characterization, but also opens a new possibility toward sideband applications.

DOI: 10.1103/PhysRevLett.127.184301

Micro- and nanomechanical resonators have been shown to be ultrasensitive for charge, force, and mass measurements in the nonlinear regime [1–6]. However, the high sensitivity also renders the resonators susceptible to environmental fluctuations such as thermal noise [7–10] or molecular motion [11,12], thereby limiting their applications. One way to circumvent this limit is by taking advantage of squeezing effects, where the fluctuation of one quadrature is reduced at the expense of that in its conjugate [13]. Such a signature was firmly established in both theory and experiment to characterize squeezing effects in various types of resonators [14–17]. However, the squeezing effect in the quadrature is usually very subtle and requires sensitive measurements and careful analysis to enable its detection, particularly in systems of high quality factors (Q).

Recently, there has been rising interest in the sideband response of resonantly driven nonlinear modes [18–20]. Nonlinear effects are significant in resonance-based sensors, and they give rise to interaction between different vibration modes [21–23] and frequency mixing [24–29], leading to interesting sideband phenomena. Huber *et al.* [18] recently revealed that the fluctuations around stable states of the driven system can also result in sideband response. They appear in pairs at either side of the drive frequency and exhibit a strong amplitude asymmetry. More importantly, their integrated intensity ratios give direct access to squeezing in the system [18], which avoids the difficulties in the quadrature method. On the other hand, these sidebands also have important implications in technological applications, such as tunable signal-to-noise ratio amplifiers, supernarrow frequency detectors, and filters [30]. Therefore, it is of great importance to understand their behavior under external stimulus and achieve the control of these sidebands.

In this Letter, we present a so-far undescribed sideband response of a nonlinear vibrating membrane resonator using a two-tone measurement. In addition to the drive tone that resonantly excites the system, we also apply an additional probe tone with a very low frequency (< 1 kHz). We find that this probe tone modulates the eigenfrequency of the system and leads to a sideband response markedly different from previous studies [18–20]. Specifically, both their amplitudes and line shapes show strong asymmetries and, most saliently, the sidebands exhibit a typical antiresonance response. We further show that the antiresonance frequency can be used to determine the squeezing parameters of the system, and they are tunable through the control of vibrational states of the driven mode, which provides a wide tunability for the sideband applications mentioned above [30]. In addition, since parametric modulation is widely used in different areas [17], such as coupling of mechanical resonators [31,32], parametrons [20], and optomechanics [33], our results can be adapted to many different systems. Finally, they may also give insight into other sideband related phenomena, such as the energy transfer via mode coupling in the nonlinear and the chaotic regime [20,26,32,34,35].

The measured device is composed of a ∼500 nm thick rectangular ($542 \times 524\ \mu m^2$) silicon nitride (Si-N) membrane suspended on a massive silicon frame attached to a piezo ring. The vibration of the freestanding membrane is excited by applying an ac voltage onto the piezo ring at a drive frequency f_d close to the eigenfrequency f_0 of the membrane resonator.

To detect the vibrations, we fabricate 27 nm thick aluminum structures on the membrane using a standard e-beam lithography technique and measure the inductive voltage across the structures (with 30 μm effective length, perpendicular to the magnetic field) under an external uniform magnetic field, as depicted in Fig. 1(a). Voltage

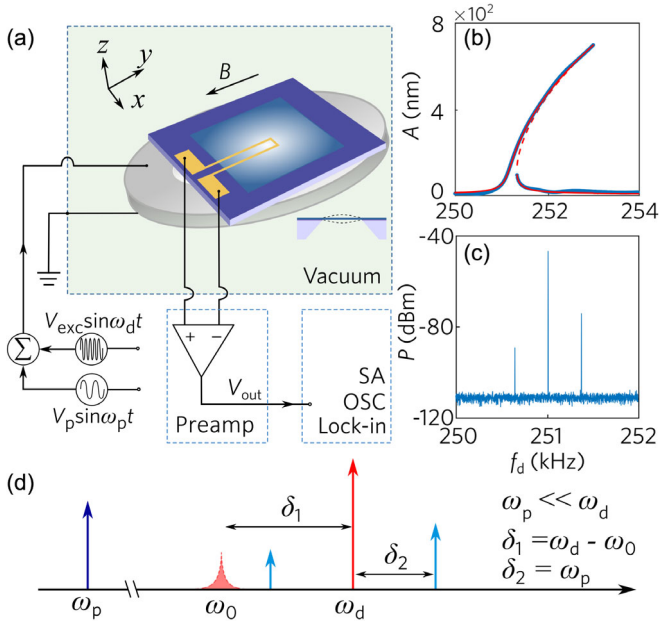

FIG. 1. (a) Schematic drawing of the Si-N membrane resonator structures (cross section shown as inset) and the on-chip electromagnetic detection scheme. (b) The frequency response curve of the fundamental (1,1) mode (solid blue line) measured at $V_{\rm exc} = 0.1$ V fitted by the Duffing model (red dashed line). (c) The measured power spectrum of a two-tone experiment with $f_d = 251$ kHz and $V_{\rm exc} = 0.5$ V, $f_p = 380$ Hz and $V_p = 0.3$ V. (d) Schematic drawing of the measurement scheme and the frequency relation between the drive and probe tone and their response.

signals are captured by the differential preamplifier to suppress the common-mode noise before measurements. The real vibrational amplitude can be quantitatively obtained from the voltage using Faraday's law. All the measurements are performed in vacuum at room temperature. More details about the sample fabrication, setup details, and fitting processes can be found in the Supplemental Material [36] and also in our previous works [37–39].

Figure 1(b) shows the response of our system to a typical single excitation $V_{\rm exc}(t) = V_{\rm exc}\sin(2\pi f_d t)$ driven close to its fundamental mode. The vibration exhibits a typical Duffing (i.e., geometric cubic nonlinearity) response with two stable states of different vibration amplitudes when the drive tone is swept along different directions. We can quantitatively extract the driven-mode parameters, including its eigenfrequency $f_0 \approx 250.85$ kHz, damping $\Gamma/2\pi = 13.5$ Hz ($Q \approx 18000$) and the cubic (Duffing) nonlinearity $\beta = 1.13 \times 10^{23}$ m^{-2} s^{-2} using the methods described in the Supplemental Material [36]. In the upper branch (i.e., the large vibration state), a simultaneous application of a drive tone at f_d and a probe tone with a much smaller frequency f_p can result in the excitation of two ultranarrow side peaks with their frequency at $f_d + f_p$ (blue side peak) and $f_d - f_p$ (red side peak), respectively, as indicated by our experiments in Fig. 1(c). These frequency relations are schematically summarized in Fig. 1(d). From here, we can safely exclude the possibility of a side peak induced by cubic nonlinearity, where the side peak should locate at 2 times the probe frequency away from the drive frequency [40].

We then sweep the probe tone from 10 to 1000 Hz with a step size of 10 Hz under a fixed drive tone, and the sideband response is plotted in Fig. 2(a). Their amplitude reaches a maximum at a peak frequency $f_{\rm pk} = \pm 380$ Hz and starts to decrease if f_p further increases. More importantly, there is a prominent silent region where the sideband signals are strongly suppressed below the noise floor. This region only appears in the red sideband, but is absent in the blue sideband, leading to a drastically asymmetric line shape. We will show below that there exists a minimum point M in the silent region with its frequency and amplitude labeled by $f_{\rm ar}$ and $P_{\rm ar}$, respectively. The sidebands also exhibit interesting phase response as depicted by the blue dots in Fig. 2(b). There are phase shifts of π when the ultranarrow side peaks are tuned through the drive tone f_d, the two sideband peaks at $f_d \pm f_{\rm pk}$, and the M point at $f_d + f_{\rm ar}$. All these features in both the amplitude and phase are reminiscent of a typical antiresonance response [41,42]. In the Supplemental Material [36], we show that the piezo can be excluded as a possible origin of the antiresonance. We also show additional sideband spectra measured under different drive conditions and from another device, all exhibiting similar response.

To model the observed sideband response, we use the following equation of motion:

$$\ddot{x} + 2\Gamma\dot{x} + [\omega_0^2 - a^2\cos(\omega_p t)]x + \beta x^3 = F\cos(\omega_d t), \quad (1)$$

where F, $\omega_0 = 2\pi f_0$, $\omega_d = 2\pi f_d$, and $\omega_p = 2\pi f_p$ denote the driving force, angular frequency of the flexural mode, drive tone, and probe tone, respectively. The probe tone also modulates the eigenfrequency with a strength of a^2, which can be characterized via a dc measurement with the method in the Supplemental Material [36].

Using the standard rotating wave approximation [18,43], we can switch from the lab frame into the rotating frame with two new quadratures y and y^*. We can approximate the solution by expanding the quadrature y into a main response y_0 and the perturbed response y_1. The former describes the response at ω_d, while the latter is responsible for the sidebands. We find that y_0 is governed by the well-known Duffing equation, and the equation of motion for y_1 is

$$\dot{y_1} = -\Gamma(1 + i\delta\omega - 2i|y_0|^2)y_1 + i\Gamma y_0^2 y_1^* - i\Gamma\cos(\omega_p t)y_0, \quad (2)$$

with $\delta\omega = (\omega_d - \omega_0)/\Gamma$. Here, the first two terms on the right-hand side of the equation describe the vibrations when the resonator deviates from the stable states and the last term

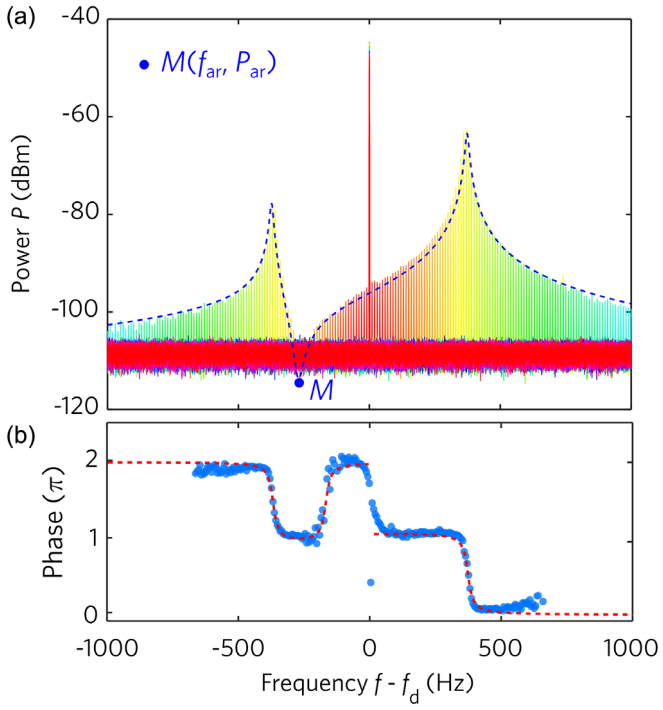

FIG. 2. (a) Overlaid power spectra with a sweeping probe frequencies f_p increasing from 10 to 1000 Hz in steps of 10 Hz and $V_p = 0.5$ V under a given drive $V_{\mathrm{exc}} = 0.5$ V and $f_d = 251$ kHz. The color coding indicates different probe frequencies. The blue dashed line shows a parameter-free sideband calculation using Eq. (1). The coordinate $M(f_{\mathrm{ar}}, P_{\mathrm{ar}})$ marks the calculated minimum point of the silent region. (b) The phases of the sideband captured under the same condition in (a) and the calculated phase are shown in blue dots and red-dashed line, respectively. (a) and (b) share the same frequency axis.

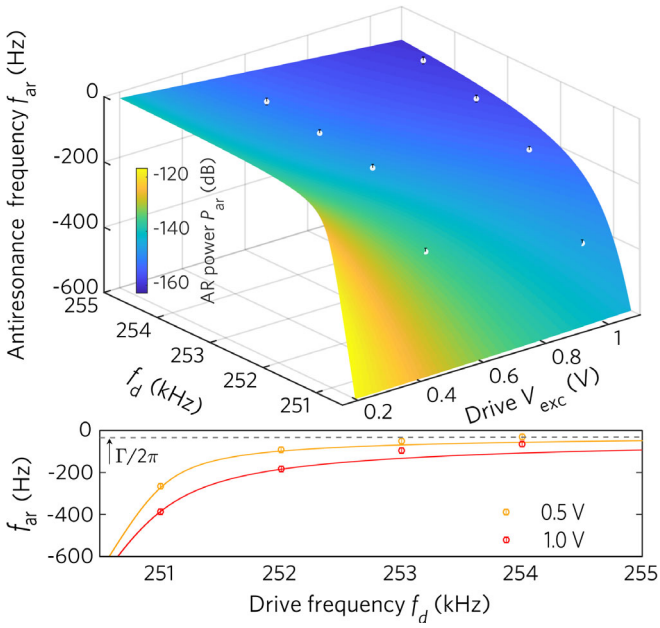

FIG. 3. Theoretically calculated antiresonance frequencies f_{ar} and their power P_{ar} under different drive frequency f_d and power V_{exc}. The white spheres are the experimentally extracted f_{ar} at drive strength (0.5 and 1.0 V) and different fixed f_d with an error bar of ± 10 Hz. The lower panel shows line cuts for two fixed voltages comparing the model (lines) and the experimental results (dot).

represents a force induced by the parametric modulation. By solving this equation, we obtain the sideband amplitudes as well as their phases at different probe frequencies. Further details of the theoretical calculation can be found in the Supplemental Material [36].

In Figs. 2(a) and 2(b), we compare the theoretical calculations (dashed lines) with experiment data of the amplitude and phase of the sideband response, respectively, and they both showed excellent agreements. We note that the π phase shift across the drive frequency is not an intrinsic effect but due to a phase delay between the longitudinal and transverse waves in the piezo [44]. Further discussion can be found in the Supplemental Material [36].

From here, we can clearly see that the silent region in experiment corresponds to an antiresonance dip M in the sideband response. In fact, the emergence of a clear antiresonance dip requires $\omega_{\mathrm{pk}}/\Gamma \gg 1$, and in this weak damping limit [45], we find that f_{ar} can be well approximated by

$$\omega_{\mathrm{ar}} = \Gamma\sqrt{1 + (\delta\omega - |y_0|^2)^2}. \tag{3}$$

This relation suggests that the position of the M point is susceptible to the vibration state of the driven mode, as y_0 is determined by both the drive and the detuning of the drive tone (see Supplemental Material [36]).

Figure 3 shows the calculated f_{ar} and P_{ar} as a function of power and detuning of the drive tone using the mode parameters given above. To compare with experiments, we can extract f_{ar} using the center frequency of the silent region, and the error bars correspond to the width of the silent region [46]. These experimentally extracted positions (white spheres) agree well with our theoretical calculation, as indicated in the lower panel of Fig. 3. We note that when the excitation is strong, nonlinear effects beyond the Duffing model [26,34] could come into play and lead to a small but noticeable deviation in the 1 V data (see Supplemental Material [36]). We can also make the following observations: (1) The highest power in the calculations here is still 10 dBm less than our experimental noise level, indicating an excellent cancellation effect of the sideband motion. (2) It is also evident here that f_{ar} has a lower bound given by the damping $\Gamma/2\pi$, as suggested from Eq. (3). (3) When the power of the drive tone is large or its detuning is small, f_{ar} is significantly away from the drive frequency.

Further insights can be gained by comparing our results with the sidebands induced by thermal fluctuations [18]. In Fig. 4(a), we compare a theoretical sideband spectrum of our case (red line) with that by thermal fluctuation (black

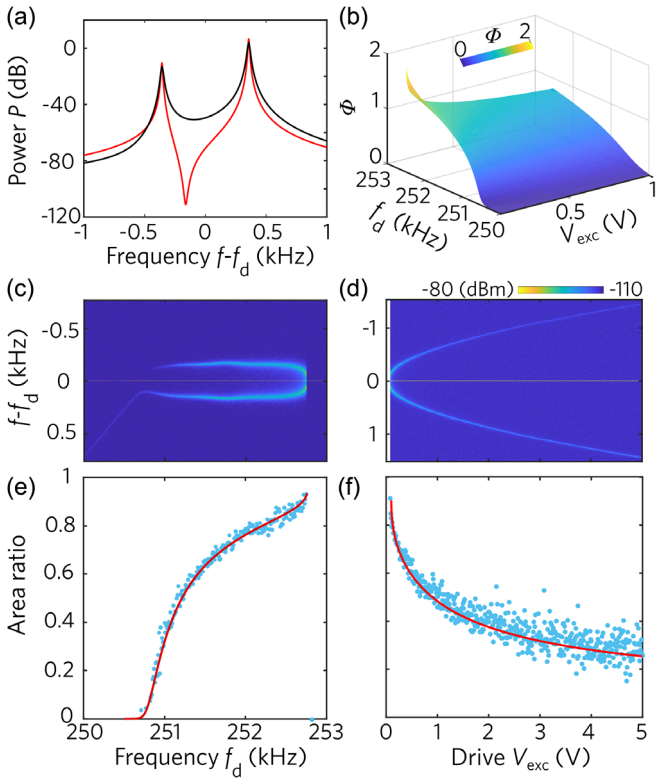

FIG. 4. (a) Theoretical sideband amplitudes driven by broadband noise (black) and a probe tone (red) with the same drive tone. (b) Calculated squeezing parameter ϕ using f_{ar} under different drive conditions. (c) Detuning-dependent sidebands measured with $V_{\mathrm{exc}} = 0.1$ V. (d) Drive-dependent sidebands measured at $f_d = 252.5$ kHz. (e) The intensity area ratio between the left and the right sideband I_-/I_+ of (c). (f) The I_-/I_+ of (d). In both (c) and (d), the noise bandwidth is 300 kHz and $V_{\mathrm{noise}} = 0.4$ V. The theoretical results from our model are shown as red solid lines and the experiments are shown as blue dots, and they share the same y axis. (c),(e) and (d),(f) pairwise share the same x axis.

line), both using the mode parameters from our experiments. Except for the antiresonance feature, the two spectra have very similar line shapes, particularly regarding the peaks. Therefore, both types of sidebands reflect the vibration modes around the stable states of the driven mode (i.e., sideband). The peak positions of the sidebands correspond to the eigenfrequency of these vibration modes and can be determined by

$$\omega_{\mathrm{pk}} = \Gamma \cdot \mathbf{Im}\left(\sqrt{(3|y_0|^2 - \delta\omega)(|y_0|^2 - \delta\omega)}\right), \qquad (4)$$

where **Im** indicates the imaginary part of the argument. The emergence of an antiresonance in the sideband spectrum reveals the different character of the drive forces: a deterministic coherent single-frequency force that periodically changes the system parameters (appearing as combined amplitude-frequency modulation here, see Supplemental Material [36] and Refs. [47,48]) destructively interferes with sidebands, while this effect is absent in the sidebands induced by broadband stochastic noise. Based on this observation, these sidebands can be delineated as "quasimodes" characterized as eigenstates controlled by the vibration states of the mechanical system in the nonlinear regime.

Even though the sidebands induced by parametric modulation are deterministic, we can nevertheless relate them with the squeezing effect of the fluctuations in the system. In the weak damping limit, there is a simple connection between the squeezing parameter ϕ that measures the transfer of fluctuations between a pair of conjugate variables and the antiresonance frequency in the spectrum,

$$\tanh 2\phi = \frac{\omega_{\mathrm{ar}} + \Gamma\delta\omega}{2\omega_{\mathrm{ar}} + \Gamma\delta\omega}. \qquad (5)$$

We note that the above relation only applies when the system is in the upper branch. In principle, a similar expression for the lower branch can be derived. However, in the experiment, it is difficult to identify an antiresonance structure in the sideband spectrum due to its low amplitude (see Supplemental Material [36]). We also note that, from Eq. (5), the squeezing parameter ϕ only depends on the vibrational state parameters, such as detuning, damping, and normalized amplitude, but not on the external perturbation.

To testify the above relations, we compare the squeezing parameters extracted from antiresonance frequency and those from the noise-induced sideband area ratio. For a thermally induced sideband, it has been shown that the integrated intensity ratio between the two sidebands (I_-/I_+) is solely determined by the squeezing parameter ϕ [18]. Because of a moderate Q in our device, the environmental thermal fluctuation itself does not induce detectable sidebands. Nevertheless, we can still access this quantity by introducing a broadband white noise of 300 kHz bandwidth and $V_{\mathrm{noise}} = 0.4$ V [36] in addition to a drive tone of $V_{\mathrm{exc}} = 0.1$ V and $f_d = 252.5$ kHz, shown in Figs. 4(c) and 4(d). The integrated intensity can be obtained by fitting the sidebands around the peak frequency with two independent Lorentzian functions. Figures 4(e) and 4(f) show the detuning and drive power dependence of the integrated intensity ratio in blue dots, while the red lines in Figs. 4(e) and 4(f) denote the theoretical calculated values using f_{ar} [Eqs. (3) and (5)]. We emphasize that there is no free parameter used in these calculations and the excellent agreement between the two methods indicates that f_{ar} is indeed a reliable indicator of the squeezing parameter.

Finally, we wish to comment on the robustness and simplicity of our method. In the previously reported method [18], a separate fitting is required for every

sideband spectrum to extract the squeezing parameter. In contrast, our antiresonance frequency method only relies on the knowledge of three parameters: $\delta\omega$, Γ, and ω_{ar}, all of which can either be directly extracted from the experiment or from a one-time fitting with the driven modes, making our method much easier and simpler. The antiresonance frequency also provides a direct way to compare the squeezing parameters under different conditions. Figure 4(b) shows the calculated ϕ over the same parameter space as that in Fig. 3, and it is positively related to both the detuning and force. By comparing this result to the f_{ar} map in Fig. 3, we can deduce that the distance between f_{ar} and the drive frequency is inversely related to ϕ: the smaller the distance, the larger ϕ.

In conclusion, we measured the sideband response of a free-standing Si-N membrane using a two-tone measurement under the conditions that (1) it is in the strongly vibrating state of its nonlinear regime and (2) its eigenfrequency is modulated at a low frequency. We observed typical antiresonance line shapes in the sideband spectra. The amplitude and the phase of these sidebands can be well described by a Duffing equation with its eigenfrequency being parametrically modulated at the probe-tone frequency. The antiresonance results from a destructive interference between the probe tone and the resulting sideband. We further demonstrate that the antiresonance can be controlled by the vibrational state of the driven mode, thus providing a new possibility for future application of sidebands. For example, these sidebands can act as quasimodes and couple with other vibrational modes for energy reshuffling in a nonlinear system. Finally, we provide a robust and simple method to characterize the squeezing effect even for resonators with a moderate Q, evidenced by the excellent agreement between the squeezing parameter extracted with the antiresonance frequency and those with the sideband-area method.

The authors thank J. Boneberg for help with the experimental setups. We are indebted to J. S. Ochs, E. M. Weig, G. Rastelli, and W. Belzig for fruitful discussion and comments about the work. The authors gratefully acknowledge financial support from the China Scholarship Council, the A. v. Humboldt Foundation, the Deutsche Forschungsgemeinschaft (DFG, German Research Foundation) through SFB 1432 (Project-ID 425217212), and the Wisconsin Alumni Research Foundation (WARF) via the Accelerator Program.

F. Y. and M. F. contributed equally to this work.

*yuxuan.jiang@ahu.edu.cn
†elke.scheer@uni-konstanz.de

[1] Y. Tadokoro and H. Tanaka, Phys. Rev. Applied **15**, 024058 (2021).
[2] L. Papariello, O. Zilberberg, A. Eichler, and R. Chitra, Phys. Rev. E **94**, 022201 (2016).
[3] L. Li, H. Liu, M. Shao, and C. Ma, Micromachines **12**, 178 (2021).
[4] Y. Zhang, R. Kondo, B. Qiu, X. Liu, and K. Hirakawa, Phys. Rev. Applied **14**, 014019 (2020).
[5] H. Kim, J. Park, Z. Aksamija, M. Arbulu, and R. H. Blick, Phys. Rev. Applied **6**, 064031 (2016).
[6] J. Park, Z. Aksamija, H.-C. Shin, H. Kim, and R. H. Blick, Nano Lett. **13**, 2698 (2013).
[7] Y. Wen, N. Ares, F. Schupp, T. Pei, G. Briggs, and E. Laird, Nat. Phys. **16**, 75 (2020).
[8] A. Cleland and M. Roukes, J. Appl. Phys. **92**, 2758 (2002).
[9] M. Sansa, E. Sage, E. C. Bullard, M. Gély, T. Alava, E. Colinet, A. K. Naik, L. G. Villanueva, L. Duraffourg, M. L. Roukes *et al.*, Nat. Nanotechnol. **11**, 552 (2016).
[10] R. J. Dolleman, P. Belardinelli, S. Houri, H. S. van der Zant, F. Alijani, and P. G. Steeneken, Nano Lett. **19**, 1282 (2019).
[11] Y. Yang, C. Callegari, X. Feng, and M. Roukes, Nano Lett. **11**, 1753 (2011).
[12] J. Atalaya, A. Isacsson, and M. I. Dykman, Phys. Rev. B **83**, 045419 (2011).
[13] D. Rugar and P. Grütter, Phys. Rev. Lett. **67**, 699 (1991).
[14] E. E. Wollman, C. Lei, A. Weinstein, J. Suh, A. Kronwald, F. Marquardt, A. A. Clerk, and K. Schwab, Science **349**, 952 (2015).
[15] F. Lecocq, J. B. Clark, R. W. Simmonds, J. Aumentado, and J. D. Teufel, Phys. Rev. X **5**, 041037 (2015).
[16] J.-M. Pirkkalainen, E. Damskägg, M. Brandt, F. Massel, and M. A. Sillanpää, Phys. Rev. Lett. **115**, 243601 (2015).
[17] M. Dykman, *Fluctuating Nonlinear Oscillators: From Nanomechanics to Quantum Superconducting Circuits* (Oxford University Press, New York, 2012).
[18] J. S. Huber, G. Rastelli, M. J. Seitner, J. Kölbl, W. Belzig, M. I. Dykman, and E. M. Weig, Phys. Rev. X **10**, 021066 (2020).
[19] J. S. Ochs, M. Seitner, M. I. Dykman, and E. M. Weig, Phys. Rev. A **103**, 013506 (2021).
[20] T. L. Heugel, O. Zilberberg, C. Marty, R. Chitra, and A. Eichler, arXiv:2103.02625.
[21] S. Houri, D. Hatanaka, M. Asano, R. Ohta, and H. Yamaguchi, Appl. Phys. Lett. **114**, 103103 (2019).
[22] A. Ganesan, C. Do, and A. Seshia, Phys. Rev. Lett. **118**, 033903 (2017).
[23] D. A. Czaplewski, C. Chen, D. Lopez, O. Shoshani, A. M. Eriksson, S. Strachan, and S. W. Shaw, Phys. Rev. Lett. **121**, 244302 (2018).
[24] F. Braakman, D. Cadeddu, G. Tütüncüoglu, F. Matteini, D. Rüffer, A. Fontcuberta i Morral, and M. Poggio, Appl. Phys. Lett. **105**, 173111 (2014).
[25] A. Erbe, H. Krömmer, A. Kraus, R. Blick, G. Corso, and K. Richter, Appl. Phys. Lett. **77**, 3102 (2000).
[26] F. Yang, F. Hellbach, F. Rochau, W. Belzig, E. M. Weig, G. Rastelli, and E. Scheer, Phys. Rev. Lett. **127**, 014304 (2021).
[27] J. D. P. Machado and Y. M. Blanter, Phys. Rev. A **94**, 063835 (2016).
[28] D. Ramos, I. W. Frank, P. B. Deotare, I. Bulu, and M. Lončar, Appl. Phys. Lett. **105**, 181121 (2014).

[29] T. F. Roque, F. Marquardt, and O. M. Yevtushenko, New J. Phys. **22**, 013049 (2020).
[30] M. I. Dykman, D. G. Luchinsky, R. Mannella, P. V. E. McClintock, N. D. Stein, and N. G. Stocks, Phys. Rev. E **49**, 1198 (1994).
[31] J. P. Mathew, R. N. Patel, A. Borah, R. Vijay, and M. M. Deshmukh, Nat. Nanotechnol. **11**, 747 (2016).
[32] A. Keşkekler, O. Shoshani, M. Lee, H. S. van der Zant, P. G. Steeneken, and F. Alijani, Nat. Commun. **12**, 1099 (2021).
[33] M. Aspelmeyer, T. J. Kippenberg, and F. Marquardt, Rev. Mod. Phys. **86**, 1391 (2014).
[34] F. Yang, F. Rochau, J. S. Huber, A. Brieussel, G. Rastelli, E. M. Weig, and E. Scheer, Phys. Rev. Lett. **122**, 154301 (2019).
[35] S. Houri, M. Asano, H. Yamaguchi, N. Yoshimura, Y. Koike, and L. Minati, Phys. Rev. Lett. **125**, 174301 (2020).
[36] See Supplemental Material at http://link.aps.org/supplemental/10.1103/PhysRevLett.127.184301 for details of the sample preparation and measurement methods, calibration and characterization measurements of the membrane under study, examples of noise-induced sidebands in different nonlinear vibrational states, direct optically measured amplitude modulation, a detailed description of the theoretical model, and the theoretically calculated detuning and drive-dependent sidebands.
[37] F. Yang, R. Waitz, and E. Scheer, arXiv:1704.05328.
[38] R. Waitz, S. Nößner, M. Hertkorn, O. Schecker, and E. Scheer, Phys. Rev. B **85**, 035324 (2012).
[39] R. Waitz, C. Lutz, S. Nößner, M. Hertkorn, and E. Scheer, Phys. Rev. Applied **3**, 044002 (2015).
[40] R. B. Reichenbach, M. Zalalutdinov, K. L. Aubin, R. Rand, B. H. Houston, J. M. Parpia, and H. G. Craighead, J. Microelectromech. Syst. **14**, 1244 (2005).
[41] C. Sames, H. Chibani, C. Hamsen, P. A. Altin, T. Wilk, and G. Rempe, Phys. Rev. Lett. **112**, 043601 (2014).
[42] F. Wahl, G. Schmidt, and L. Forrai, J. Sound Vib. **219**, 379 (1999).
[43] A. H. Nayfeh and D. T. Mook, *Nonlinear Oscillations* (John Wiley & Sons, New York, NY, 2008).
[44] A. N. Cleland, *Foundations of Nanomechanics: From Solid-State Theory to Device Applications* (Springer Science & Business Media, New York, 2013).
[45] Note that here the weak damping limit adopts the requirement of a squeezing parameter in the following discussion for simplification.
[46] The dip position can be measured directly if the signal is strong enough, see [36].
[47] P. F. Pai and A. N. Palazotto, Mech. Syst. Signal Process. **22**, 1107 (2008).
[48] B. C. Moore and A. Sek, J. Acoust. Soc. Am. **92**, 3119 (1992).